Reduction in Earth's carbon budget imbalance

Sudhanshu Pandey, Frédéric Chevallier, Christian Rödenbeck, Brendan Byrne, Abhishek Chatterjee, Junjie Liu, Christian Frankenberg

nature communications

Article

https://doi.org/10.1038/s41467-025-61588-2

Reduction in Earth's carbon budget imbalance

Received: 26 September 2024

Accepted: 25 June 2025

Published online: 24 July 2025

Check for updates

Sudhanshu Pandey[1] ✉, Frédéric Chevallier[2], Christian Rödenbeck[3], Brendan Byrne[1], Abhishek Chatterjee[1], Junjie Liu[1,4] & Christian Frankenberg[1,4]

The Global Carbon Project (GCP) compiles an updated global carbon budget each year, synthesizing state-of-the-art estimates of anthropogenic CO_2 emissions, land and ocean sinks, and the atmospheric CO_2 growth rate. The residual between these terms, referred to as the global carbon budget imbalance, reflects the aggregate inaccuracies of the individual component estimates. Growth rates derived from marine boundary layer (MBL) surface flask mixing ratio observations are assumed to be highly accurate. Hence, land and ocean sink estimates from process models are viewed as the primary source of the imbalance. Here we show that substantial discrepancies arise when marine boundary layer growth rate estimates are used to represent the whole atmosphere. Correcting for this discrepancy using atmospheric flux inversion estimates reduces the 0.76 petagrams of carbon per year (PgC yr^{-1}) root-mean-square (RMS) imbalance (from the 2023 GCP report) by up to 25%. Further investigation into the imbalance metric between the 2017 and 2023 GCP reports shows a reduction in imbalance resulting from updates to each carbon budget component, leading to a 16% overall reduction. These reductions provide quantitative evidence of improvements in process models and inventory emission estimates, driven by enhanced forcing data and the inclusion of new carbon cycle processes. Overall, we report a 37% reduction in the root-mean-square imbalance, from 0.91 to 0.57 PgC yr^{-1}, between the 2017 and 2023 GCP reports by combining process model and inventory improvements with atmospheric growth rate corrections. Our findings indicate that land and ocean process models are more accurate than previously believed and that the scientific understanding of Earth's carbon cycle is improving.

Accurate quantification of anthropogenic carbon dioxide (CO_2) emissions and their redistribution among Earth's major carbon reservoirs (atmosphere, oceans, and terrestrial biosphere) is essential for tracking mitigation progress, informing climate policy, and projecting future climate trajectories[1–3]. As global temperatures rise and the impacts of climate change intensify, the scientific community is refining observational and modeling tools to constrain each component of the carbon cycle. The Paris Agreement's five-year Global

[1]Jet Propulsion Laboratory, California Institute of Technology, Pasadena, CA, USA. [2]Laboratoire des Sciences du Climat et de L'Environnement, LSCE/IPSL, CEA-CNRS-UVSQ, Université Paris-Saclay, Gif-sur-Yvette, France. [3]Max Planck Institute for Biogeochemistry, Jena, Germany. [4]Division of Geological and Planetary Sciences, California Institute of Technology, Pasadena, CA, USA. ✉e-mail: sudhanshu.pandey@jpl.nasa.gov

Stocktake further heightens this urgency by requiring transparent, robust assessments of carbon sources and sinks to underpin effective policy-making. Yet persistent, poorly understood variability within the natural carbon cycle still hampers the verification of reported emission reductions under international accords.

Over the past decade, researchers have addressed these shortcomings by acquiring higher-quality observations and activity data, expanding model ensembles, refining parameterizations, and incorporating previously omitted processes—such as cement carbonation and coupled nitrogen–phosphorus dynamics—into land and ocean carbon models[4–7]. These advances, which we collectively term *bottom-up* improvements, improve the process models (land and ocean uptake) and inventories (anthropogenic emissions) that underpin contemporary carbon budgets. Although such improvements should, in principle, reduce component-level errors, quantitative evidence of an overall gain in accuracy remains elusive.

CO_2 is emitted into the atmosphere due to fossil fuel combustion, industrial processes, and land-use changes. Natural sinks partially offset these emissions with ~25% uptake by oceans and 30% uptake by terrestrial ecosystems, with the remaining 45% accumulating in the atmosphere[7]. On a global scale, a mass balance exists between annual emissions, sinks, and the CO_2 annual growth rate in the atmosphere. The residual imbalance, B_I, quantifies our inability to close the budget of fluxes across the Earth's carbon cycle pools:

$$B_I = \underbrace{E_F + E_L}_{sources} - \underbrace{(S_O + S_L + S_C)}_{sinks} - G_A \quad (1)$$

All quantities on the equation's right-hand side denote the component flux estimates in petagram carbon per year (PgC yr^{-1}). E_F represents fossil fuel and industrial process emissions, E_L denotes land-use change emissions, S_O and S_L are the oceanic and land uptake, respectively, and S_C symbolizes cement carbonation[5]. G_A denotes the atmospheric growth rate of CO_2[8], caused by differences between emissions and sinks. The imbalance quantifies the sum of errors in all flux components on the right-hand side, serving as a metric for data imperfections and gaps in our understanding of the contemporary carbon cycle.

Growth rates derived from marine boundary layer (MBL) CO_2 surface flask (sometimes referred to as in situ measurements) mixing ratio measurements are typically considered highly accurate. Consequently, the budget imbalance has often been attributed primarily to inaccuracies in other components, particularly land and ocean sinks[3,7–9]. However, the atmospheric growth rate is not directly measured in units of mass change (PgC yr^{-1}) but is derived from mixing ratio measurement changes (ppm yr^{-1}) assuming instantaneous mixing of the fluxes throughout the whole atmosphere. Although surface flask measurements of atmospheric mixing ratios are very accurate and precise, errors are introduced in estimating the whole-atmosphere growth rate due to the sparsity of the MBL surface flask measurement data and methodological assumptions[7,10].

Here, we investigate the evolution of collective accuracy using the carbon-budget imbalance reported annually by the Global Carbon Project (GCP). We also quantify the error introduced when the MBL CO_2 growth rate is used as a proxy for the whole-atmosphere growth rate. We find that accounting for the discrepancy between MBL and whole-atmosphere growth rates markedly reduces the root-mean-square (RMS) of the annual imbalance time series relative to the values reported in recent GCP Carbon Budget assessments. We further assess the impact of updates to individual budget components between the 2017 and 2023 GCP reports, demonstrating that the overall accuracy of Earth's carbon-budget components has improved over this period.

Results

Whole-atmosphere growth rate correction

The GCP uses growth rate estimates from the US National Oceanic and Atmospheric Administration (NOAA) Global Monitoring Laboratory, calculated from CO_2 mixing ratio observations of well-mixed background air at MBL surface measurement stations. These growth rate estimates serve as the benchmark for most scientific and agency assessments. NOAA estimates the growth rate by smoothing data over time for each MBL station and then averaging it across latitude bands[11]. GCP converts NOAA growth rate (ppm yr^{-1}) values into the whole-atmosphere mass change (PgC yr^{-1}) using a conversion factor[12] of 2.124 PgC ppm^{-1}. This conversion assumes instantaneous mixing—an approximation that introduces errors from finite and varying atmospheric transport timescales and sparse spatiotemporal sampling of MBL observations[10]. Although the troposphere, which contains about 80% of atmospheric molecules, mixes well within a year, the stratosphere exchanges air slowly with the troposphere over a period ranging from 2–4 years[13,14].

Observed stratospheric CO_2 mixing ratios are 3–5 ppm lower than tropospheric values, reflecting slow stratosphere–troposphere exchange[14,15]. Consequently, surface-driven CO_2 increases lag in the stratosphere, creating a deficit relative to tropospheric values (see Methods). The GCP acknowledges that using a constant conversion factor of 2.124 PgC ppm^{-1}, an approximation that assumes instantaneous whole-atmosphere mixing, introduces a non-negligible source of uncertainty[7]. The error introduced by using constant conversion factors to calculate whole-atmosphere growth rates from MBL data can be broken into two errors: troposphere-sampling error and stratosphere-troposphere exchange (STE) error. The troposphere-sampling error reflects a representativeness error due to the sparsity of MBL sites.

To account for the MBL growth rate discrepancies, we compute the whole-atmosphere CO_2 growth rate using two atmospheric flux inversion models: Copernicus Atmosphere Monitoring Service (CAMS)[16] and Jena CarboScope (CS)[17]. These models optimize emissions and sinks from the oceans and land surfaces to match mixing ratio measurements at surface sites (including many MBL sites) while incorporating STE and additional atmospheric transport and sampling effects through numerical simulations nudged to meteorological reanalysis data (see Methods). Thus, the global integral of the annual net optimized surface fluxes provides the whole-atmospheric growth rate.

Alternatively, to isolate the impact of STE, we employ a simple two-box model representing the troposphere and stratosphere, assuming a 2 year STE timescale (see Methods). This model assumes MBL-derived rates perfectly represent tropospheric growth, isolating only the STE error. The Inverse models (CAMS and Jena CS) account for both troposphere sampling and STE-related errors, while the box model only accounts for the STE-related errors. Note that neither the inversions nor the box models are free of errors. However, we hypothesize that the improvements from accounting for large-scale transport effects like STE and sampling should be more significant, overall leading to a better growth rate estimate and thus reducing the imbalance.

Figure 1 presents various growth rate estimates alongside the corresponding changes in the imbalance reported by GCP in 2023. The long-term mean imbalance does not change after our corrections, but the influence of those corrections is strong during years with pronounced inter-annual variability. This is expected because the STE adjustment acts as a lagged temporal smoother on MBL growth rates when converting them to whole-atmosphere values (see Methods). Because its magnitude depends on the past values of tropospheric mixing ratios, it damps extremes and nudges annual values toward the mean (see Supplementary Section 1).

Two illustrative cases of the impact of growth rate correction are the peak imbalance of +1.7 PgC yr^{-1} in 1991 and the trough

https://doi.org/10.1038/s41467-025-61588-2

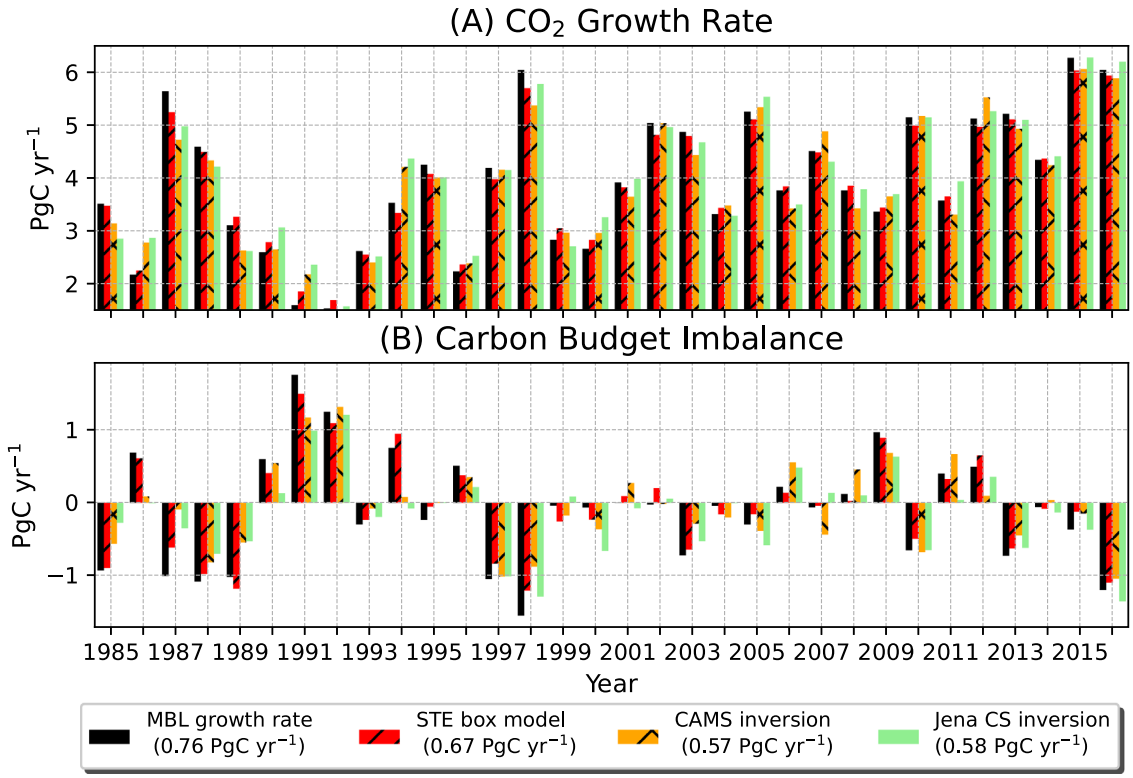

Fig. 1 | Whole-atmosphere CO_2 growth rate estimates and their corresponding carbon budget imbalance. Panel (**A**) displays the CO_2 growth rate estimates based on MBL observations from the GCP 2023 report (black bars) alongside the corrected values accounting for STE using the box model (red bars) and atmospheric flux inversions from CAMS (orange bars) and Jena CS (green bars). Panel (**B**) shows the corresponding carbon budget imbalance calculated using each CO_2 growth rate series from Panel (**A**). The RMS of imbalance is given in parentheses in the legends.

imbalance of −1.5 PgC yr^{-1} in 1998. These years coincide with the Mount Pinatubo eruption and a strong El Niño, respectively. These events induced sharp perturbations to the carbon cycle and have historically challenged bottom-up models. For 1991, the high imbalance has been linked to an underestimation of the land-sink response, likely due to a lack of representation of diffuse-radiation effects following the volcanic aerosol injection[18,19]. Our revised growth-rate estimate raises the previously low MBL value in 1991, and lowers the high value in 1998, producing a small but meaningful reduction in both imbalance extremes (CAMS imbalance for 1991 = +1.17 PgC yr^{-1} and 1998 = −0.87 PgC yr^{-1}). While these years remain prominent anomalies even after the correction, the diminished residual suggests that process models may be more skillful against such climatic shocks than previously assumed.

The annually varying corrections to the growth rate required to account for the STE effect cannot be captured by a single, time-invariant conversion factor. In particular, the widely used 2.124 PgC ppm^{-1} factor[12], derived under the assumptions of a fixed atmospheric mass and uniform, instantaneous mixing, systematically over-estimates high MBL growth years and under-estimates low MBL growth years (see Supplementary Section 1), biasing flux estimates wherever growth rates deviate from the long-term average.

The RMS imbalance in the GCP 2023 report is 0.76 PgC yr^{-1} for the period of 1985–2016. Applying the box-model-based STE correction reduces the RMS imbalance by 11% (from 0.76 PgC yr^{-1}) to 0.67 PgC yr^{-1}. The atmospheric inversion corrections from Jena CS and CAMS reduce the RMS imbalance by 24% and 25%, leading to imbalances of 0.58 PgC yr^{-1} for Jena CS and 0.57 PgC yr^{-1} for CAMS. A stronger improvement from inversions compared to box model is expected because inversions account for additional atmospheric transport dynamics and atmospheric sampling effects.

The whole-atmosphere corrections are significant relative to the budget imbalance, which aggregates the errors of all components. The growth rate correction terms themselves have RMS magnitudes of 0.16, 0.36, and 0.37 PgC yr^{-1} for the box-model, CAMS, and Jena CS estimates, respectively. For context, the largest of these correction RMS values is 49% of the GCP-2023 RMS imbalance of 0.76 PgC yr^{-1}. These improvements demonstrate that uncertainties in the atmospheric growth rate account for a substantial share of the total imbalance error. The large improvement in the imbalance due to the growth rate corrections also shows that bottom-up models are more accurate than previously perceived, based on the assumption that the imbalance was primarily caused by errors in these bottom-up models.

Improvements in process models and inventories

The GCP carbon budget estimates are updated annually to incorporate data re-evaluation and developments in process understanding, and the use of larger model ensembles[7]. Consequently, inaccuracies in budget components and the resulting imbalance are expected to decrease over time. We analyze changes in budget components between the 2017 and 2023 GCP reports to test this hypothesis. To identify the components causing the imbalance RMS reduction, we calculate an imbalance due to a component change between the 2017 and 2023 reports (see Methods), leaving other components unchanged.

Figure 2 shows the time series of carbon-flux components and the MBL CO_2 growth rate from the 2017 and 2023 GCP reports[7,8]. All components exhibit changes between the 2017 and 2023 estimates, with the largest RMS differences observed in the land-use change (0.23 PgC yr^{-1}), the land sink (0.25 PgC yr^{-1}), and the ocean sink (0.22 PgC yr^{-1}). Fossil-fuel emissions and the MBL growth rate also change notably, with RMS differences of 0.13 PgC yr^{-1} and 0.07 PgC yr^{-1}, respectively.

https://doi.org/10.1038/s41467-025-61588-2

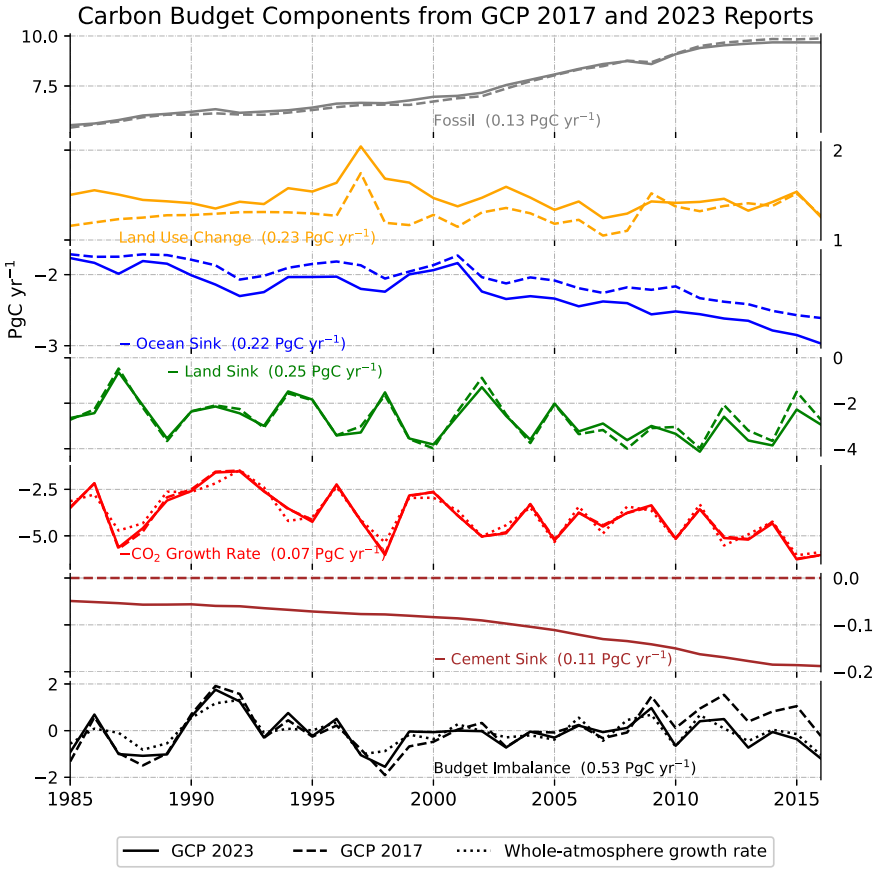

Fig. 2 | Carbon budget component estimates from the 2017 (dashed line) and 2023 (solid line) GCP reports. Negative values for ocean sink, land sink, cement carbonation sink, and MBL annual growth rate are plotted to reflect their role in the imbalance equation (Eq. 1). The dotted line in the fifth panel shows the whole-atmosphere growth rate from the CAMS inversion, and the dotted line in the bottom panel shows the resulting budget imbalance. The 2017 cement carbonation value is set to zero because cement carbonation sink was first included in the GCP 2020 report. Note that the y-axis scales of the panels differ. The values in parentheses for each panel label are the respective RMS of the difference between the GCP 2017 and 2023 time series, which gives an estimate of the magnitude of the changes.

A few reasons for the changes in the component estimates are as follows: The GCP ocean sink estimates changed between the 2017 and 2023 reports, with GCP 2023 using a combination of process models and data-driven (fCO2-based[20]) approaches (as shown in Fig. 2). NOAA MBL flask measurements were recalibrated to the 2019 WMO scale and the derived growth-rate estimates from these recalibrated mixing ratio measurement data were first used in the GCP 2021 report[6,21]. The growth rates can also change due to stabilization-latency effects in the NOAA MBL time series, which introduce a latency before convergence to the final growth rates levels (see Figure 9 of ref. 10). Beginning with the 2020 GCP report[22], the cement-carbonation sink was included after its substantial role in atmospheric CO_2 removal was recognized[5]. Between the 2017 report, in which it was not reported (i.e., assumed zero), and the 2023 report, the RMS difference in this sink is 0.11 PgC yr^{-1}, underscoring its significance.

Figure 3 presents the imbalance RMS change between the two reports. The 16% reduction in the imbalance (from 0.91 to 0.76 PgC yr^{-1}) indicates a significant decrease in the sum of errors. This reduction in imbalance is comparable to the whole-atmospheric growth rate correction when applied to the 2017 GCP report, which results in an RMS imbalance of 0.77 PgC $yr^{-1}$when using the CAMS flux inversion (see Supplementary Fig. 1). Note that applying the growth rate correction yields a smaller percentage reduction for the 2017 GCP report (a 15% drop from a 0.91 PgC yr^{-1} baseline) than for the 2023 GCP report (a 25% drop from a 0.76 PgC yr^{-1} baseline). This occurs because the total error variance, which mostly determines the RMS of the budget imbalance, is effectively the quadrature sum of variances from multiple error sources (error variances combine in quadrature if independent). Consequently, while a growth rate correction reduces the variance component associated with the growth rate, its fractional impact on the overall RMS is smaller when the initial RMS imbalance (and thus the total underlying error variance) is large due to other substantial uncorrected error components. Therefore, as bottom-up emission and sink estimates continue to improve, growth rate errors will account for an increasingly dominant share of the residual budget imbalance, underscoring the need for further refinement of observational and modeling constraints on global CO_2 growth rates.

The colored crosses (and the "+" signs) in Fig. 3 show the RMS imbalance impact due to different component updates (see Methods). We find that all carbon budget component updates lead to an imbalance reduction. This shows that the component estimates have individually improved, and the imbalance improvement is not due to a compensatory effect where the improvement of one component offsets the worsening of another.

The causes of improving estimates or error reduction can be broken into four broad effects: (1) standard error reduction due to an increase in ensemble size, (2) improvement in process representations, (3) forcing data improvement, and (4) model resolution improvement. The process level improvements stem from numerous individual advancements (see Table 3 of Friedlingstein et al.[7], Table S1 of Le Quéré et al.[8], and Sitch et al.[4]). Fossil fuel emission estimates have likely improved due to additional effect of the availability of better emission activity data from emerging economies[23].

https://doi.org/10.1038/s41467-025-61588-2

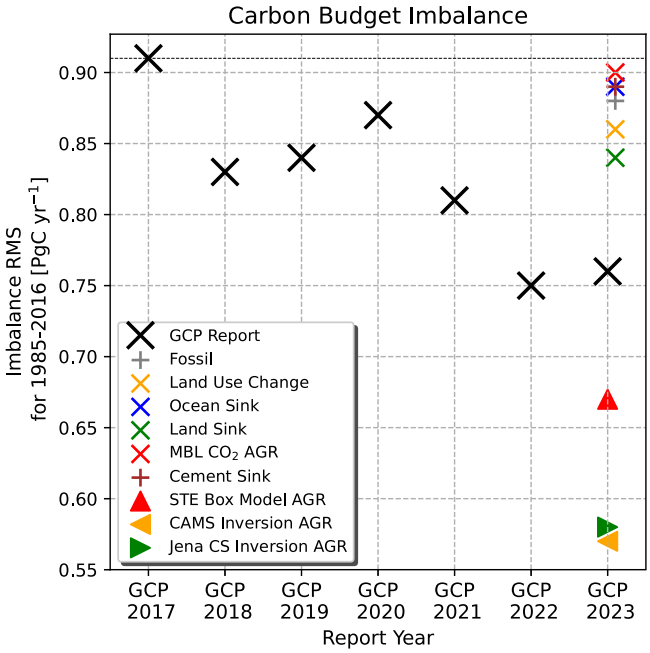

Fig. 3 | Improvements in the global carbon budget imbalance for the 1985–2016 period. The *y*-axis represents the root mean square (RMS) of the annual imbalance time series. The black crosses represent the imbalance RMS from different GCP reports (*x*-axis). The STE box model (red triangle) annual growth rate (AGR) estimates accounts for an STE time of 2 years. The growth rate estimates from the CAMS (orange triangle) and Jena CS (green triangle) atmospheric flux inversions account for troposphere-sampling errors of the MBL sites in addition to the STE. The colored symbols ("+" and "x") mark the imbalance when considering each component update between the 2017 and 2023 GCP reports, one by one, while keeping all other components unchanged from the 2017 report.

The ensemble size of models has increased. For instance, the number of Dynamic Global Vegetation Models (DGVMs) used for the land sink grew from 15 in GCP 2017 to 20 in GCP 2023, and the number of ocean–biogeochemistry models (OBGCMs) rose from 8 to 10. The number of book-keeping models for land-use change also increased from 2 to 3. The GCP 2021 report[21] started using ocean sink estimates as the mean of the estimates from the ocean process models and data-driven sink estimates using fCO_2-based SOCAT estimates. A larger ensemble to estimate a carbon cycle component can, in principle, reduce the standard error of the multi-model mean through the familiar $1/\sqrt{N}$ relationship.

The resolutions of meteorological and other forcing data, as well as of the process models, have improved. In the GCP 2023 report, ocean models included three models with 75 vertical layers, compared to a maximum of 51 layers in the GCP 2017 report. More carbon cycle processes are represented in the models used in the GCP 2023 report than in the GCP 2017 report. For example, better accounting for the diffuse radiation effect on plant productivity has been shown to significantly improve the budget imbalance during volcanic eruption years, such as the 1991 Pinatubo eruption[18,19]. In the GCP 2023 report, 6 out of 20 land sink models accounted for this effect, whereas none of the 15 land sink models did in the GCP 2017 report. Simulation of fire ignition and suppression was absent in one-third of the models in the GCP 2017 report, whereas in the GCP 2023 report, only one-fourth lacked this feature. Peat fires were included in only one land model in the GCP 2017 report, but in two models in the GCP 2023 report. Wood harvest was included in 40% of GCP 2017 DGVMs, compared to 75% of GCP 2023 DGVMs. Nitrogen fertilization was included in only 2 DGVMs in the GCP 2017 report but 10 DGVMs in the GCP 2023 report.

The carbon budget imbalance analysis presented here can serve as a diagnostic for attributing overall budget improvements to specific component changes. For instance, substituting land sink estimates in the GCP 2023 budget with those from only the six models accounting for diffuse radiation effects yields an RMS imbalance of 0.72 PgC yr^{-1}, a notable reduction from the 0.80 PgC yr^{-1} obtained using the multi-model mean from the fourteen models omitting this process (all other GCP 2023 components held constant). We also test whether increases in model ensemble sizes are a driver of the observed imbalance reduction between the 2017 and 2023 GCP reports, as larger ensembles might theoretically reduce the standard error of the multi-model mean. However, our tests indicate that, for both land and ocean sinks, expanding the ensemble size does not, in itself, lead to a reduction in the budget imbalance. The RMS imbalance for GCP 2023 using only the land sink models present in the 2017 ensemble is 0.758 PgC yr^{-1}, closely aligned with the 0.762 PgC yr^{-1} RMS imbalance using the full GCP 2023 land model ensemble; a similar outcome is observed for ocean sink estimates. While a complete imbalance attribution of all changes between the 2017 and 2023 GCP reports is not undertaken here, the budget imbalance analysis presented here can be utilized in future investigations to quantify the influence of individual modifications.

We also perform a suite of sensitivity tests (see Supplementary Section 2) to check that the declining RMS budget imbalance reported here reflects genuine component estimate improvements. We find consistent imbalance reductions across three independent periods (1960–1984, 1985–2004, and 2005–2016), further corroborating that these advances arise from better forcing data and refined process representations. In Supplementary Section 3, we discuss how the carbon budget imbalance (the net effect of all actual component errors) relates to the GCP-reported uncertainty estimates for these components.

Discussion

By integrating whole-atmosphere growth rate corrections with improvements in component models between GCP 2017 and GCP 2023 reports, we show a substantial reduction in imbalance, from 0.91 PgC yr^{-1} (the RMS imbalance of the GCP 2017 budget using its original MBL-based growth rate) to 0.57 PgC yr^{-1} (using GCP 2023 components combined with our whole-atmosphere growth rate correction from CAMS inversion), equating to a 37% imbalance reduction. We find that substantial error is introduced when MBL growth rate data are used to represent whole-atmosphere growth rate, bolstering confidence in bottom-up models by challenging the previous notion that inaccuracies in these models were the primary cause of imbalance. The whole-atmospheric growth rate correction, when applied to the 2017 GCP report, results in a similar improvement in imbalance to that achieved through the combined improvements in carbon budget components between the GCP 2017 and GCP 2023 reports. Our analysis also reveals improvements across all carbon budget components, demonstrating that not only have collective inaccuracies decreased, but individual component estimates have also advanced. The improvements in bottom-up models and inventories are likely due to the combined effects of enhanced meteorological and other forcing data, improved process understanding, and increased model resolution.

The Paris Agreement's five-year Global Stocktake necessitates urgent scientific refinement of carbon cycle understanding for effective policy-making. Currently, persistent unexplained natural carbon cycle variability hinders the verification of reported anthropogenic emission reductions under these agreements[3]. Our final RMS imbalance estimate of 0.57 PgC yr^{-1} is comparable to the GCP uncertainty estimate for global fossil fuel emissions (0.5 PgC yr^{-1}) or the emission reduction during the 2020 COVID-19

pandemic (0.55 PgC yr^{-1})[7]. This reduced imbalance, approaching the scale of annual emission uncertainties and significant emission anomalies (like the COVID-19 dip), suggests that the global carbon budget imbalance can become an increasingly powerful tool in the future to track large anthropogenic emission changes. Ultimately, our results signify an enhanced understanding and increasingly accurate representation of the Earth's carbon cycle by process models and emission inventories, which should improve future climate projections and the monitoring of anthropogenic emissions.

Methods

We analyze the global carbon budget imbalance from 1985 through 2016. The primary baseline budgets are taken from the GCP 2017[8] and GCP 2023[7] reports. The analysis starts in 1985. For inversion-based growth rates, this allows for a sufficient spin-up period (e.g., CAMS begins in 1979), accounting for typical stratosphere-troposphere exchange (STE) timescales of 2–4 years. We estimate the whole-atmosphere growth rate from a box model and as the global, annual integral of the net surface CO_2 fluxes optimized by the CAMS and Jena CS atmospheric inversion systems. The whole-atmosphere growth rate is theoretically equal to the net fluxes, which are mainly due to surface emissions and sinks, except for a minor contribution from CO oxidation.

Atmospheric inversions

CAMS. The CO_2 atmospheric inversion of the operational Copernicus Atmospheric Monitoring Service (CAMS) assimilates atmospheric mixing ratio observations (surface air-sample measurements) in the LMDz atmospheric transport model. During the assimilation process, the LMDz model is inverted in a variational framework to yield statistically optimal CO_2 surface emissions and sinks at weekly and grid-point scales. For CAMS version v22r1 used here, available surface air-sample measurements at 159 sites between January 1979 and March 2023 were assimilated; the model resolution was 79 layers in the vertical, 1.27° in latitude and 2.5° in longitude. More details on the inversion system can be found in Chevallier et al.[16], and references therein.

Jena CarboScope (CS). Atmospheric tracer transport in the Jena CarboScope inversions is simulated by the TM3 atmospheric chemical transport model at a resolution of ~4° in latitude by 5° in longitude, with 19 vertical layers driven by meteorological fields from the NCEP (National Centers for Environmental Prediction) reanalysis. The run "s76_v2023" of the Jena CarboScope employed here uses 8 atmospheric CO_2 measurement sites that span its estimation period from 1976 to 2022. CarboScope uses a fossil-fuel CO_2 emission prior from GridFED, an ocean CO_2 exchange prior based on the interpolation of SOCAT pCO_2 data. In contrast to the CarboScope run used in the GCP 2023 report, the run s76_v2023 used here has explicit interannual degrees of freedom (i.e., no regression against predictor variables). For more details on the setup, see Appendix A of[17], with slight updates described on the website of CarboScope[24].

Although the two inversions differ in aspects such as the number of assimilated measurement-site networks and vertical model resolution, they both incorporate data from a common core MBL network. This MBL network provides the primary observational constraint for estimating the annual global CO_2 growth rate in these inversions. Both inversions are designed to track the global CO_2 growth rate while also capturing key transport processes, including stratosphere-troposphere exchange.

To demonstrate that the inversions not only reproduce the MBL observations but also capture large-scale transport effects—such as the slow stratosphere–troposphere exchange—we compare the CAMS-inversion–simulated CO_2 mole fractions against NOAA MBL observations (Supplementary Fig. 2)[25] and AirCore profiles (Supplementary Fig. 3)[26]. Our analysis shows that the optimized CAMS fields reproduce the MBL mixing ratio measurements and resolve the stratosphere–troposphere CO_2 mixing ratio gradient observed by AirCore.

Two-box model

To isolate the impact of stratosphere-troposphere exchange (STE) on the inferred whole-atmosphere CO_2 growth rate, we employ a two-box model representing the troposphere and stratosphere. This model simulates the exchange of CO_2 between these two reservoirs, where air is exchanged carrying the CO_2 mixing ratio of its box of origin. The net rate of CO_2 mixing ratio change in each box is driven by the difference in their respective CO_2 mixing ratios, modulated by a characteristic exchange timescale.

Let $C_{\mathrm{tropo}}(t)$ and $C_{\mathrm{strato}}(t)$ denote the mean CO_2 mixing ratios (in ppm) in the troposphere and stratosphere, respectively, at time t. We use $K_{\mathrm{atm}} = 2.124$ PgC ppm^{-1} as the conversion factor representing the CO_2 mass required to raise the mean atmospheric mixing ratio by 1 ppm[12]. The troposphere is assumed to contain a fraction $f_{\mathrm{tropo}} = 0.8$ of the total atmospheric air mass, and the stratosphere a fraction $f_{\mathrm{strato}} = 0.2$[13].

The model dynamics are described by the following system of ordinary differential equations:

$$\frac{dC_{\mathrm{strato}}(t)}{dt} = \frac{C_{\mathrm{tropo}}(t) - C_{\mathrm{strato}}(t)}{\tau} \tag{2}$$

$$\frac{dC_{\mathrm{tropo}}(t)}{dt} = \frac{E_{\mathrm{net}}(t)}{f_{\mathrm{tropo}} K_{\mathrm{atm}}} - \frac{f_{\mathrm{strato}}}{f_{\mathrm{tropo}}} \frac{C_{\mathrm{tropo}}(t) - C_{\mathrm{strato}}(t)}{\tau} \tag{3}$$

Here, τ is the characteristic exchange timescale between the two boxes, representing the e-folding time for stratospheric mixing ratio adjustment (i.e., the stratospheric air residence time). $E_{\mathrm{net}}(t)$ (in PgC yr^{-1}) denotes the net CO_2 flux (from surface sources/sinks and atmospheric chemical production) entering the troposphere. The factor $f_{\mathrm{strato}}/f_{\mathrm{tropo}}$ in Eq. 3 ensures CO_2 mass conservation during exchange between the reservoirs with differing air masses.

Our objective is to estimate $E_{\mathrm{net}}(t)$, which serves as the box-model derived whole-atmosphere CO_2 growth rate (G_A^{box}), based on observed tropospheric CO_2 changes. Rearranging Eq. 3 yields:

$$E_{\mathrm{net}}(t) = f_{\mathrm{tropo}} K_{\mathrm{atm}} \left[\frac{dC_{\mathrm{tropo}}(t)}{dt} + \frac{f_{\mathrm{strato}}}{f_{\mathrm{tropo}}} \frac{C_{\mathrm{tropo}}(t) - C_{\mathrm{strato}}(t)}{\tau} \right] \tag{4}$$

We first estimate the time series of tropospheric CO_2 mixing ratio $C_{\mathrm{tropo}}(t)$ using the annual CO_2 growth rates from the GCP 2023 report as $\frac{dC_{\mathrm{tropo}}(t)}{dt}$ and the initial condition $C_{\mathrm{tropo}}(0) = 280$ ppm in the year 1750 ($t = 0$). The stratospheric CO_2 mixing ratio can also be expressed analytically as:

$$C_{\mathrm{strato}}(t) = e^{-t/\tau} \left[C_{\mathrm{strato}}(0) + \int_0^t \frac{e^{s/\tau}}{\tau} C_{\mathrm{tropo}}(s) ds \right] \tag{5}$$

$C_{\mathrm{strato}}(t)$ is then obtained by numerically integrating Eq. 5 initialized with $C_{\mathrm{strato}}(0) = 280$ ppm. This formulation shows that $C_{\mathrm{strato}}(t)$ depends on its initial state and past tropospheric mixing ratios. It is an exponentially weighted moving average of tropospheric mixing ratios with characteristic timescale τ. This "stratospheric memory" effect imposes a lagged temporal smoothing when inferring whole-atmosphere growth rate from tropospheric CO_2 changes. With $C_{\mathrm{tropo}}(t)$, its derivative $\frac{dC_{\mathrm{tropo}}(t)}{dt}$, and the calculated $C_{\mathrm{strato}}(t)$ (using scipy.integrate module in Python for Eq. 5), we compute $E_{\mathrm{net}}(t)$ using Eq. 4.

A STE time τ of 2 years was implemented in the box model. The simulated CO_2 mixing ratios and the resulting stratosphere-troposphere mixing ratio difference from this box model are shown in Supplementary Fig. 4. This simulated difference aligns well with observed differences from AirCore profiles and CAMS 3D mole fraction field data. Sensitivity tests assessing the influence of varying τ on the budget imbalance reduction are presented in Supplementary Table 1.

Individual component's imbalance impact

To isolate the impact of updates to an individual carbon budget component C on the overall budget imbalance, we recalculate the imbalance time series by starting with the budget imbalance from the 2017 GCP report ($B_{IM,17}$) and effectively substitute the 2017 estimate of component C (C_{17}) with its 2023 estimate (C_{23}), while keeping all other components at their 2017 values.

The resulting imbalance due to the update in the component C, denoted $B_{IM,C}$, is calculated as:

$$B_{IM,C} = B_{IM,17} + \delta_C (C_{23} - C_{17}) \quad (6)$$

Here, C_{17} and C_{23} are the multi-model mean estimates for component C from the 2017 and 2023 GCP reports, respectively. The factor δ_C is $+1$ if component C is a source term in Eq. 1 (i.e., fossil emissions E_F or land-use change emissions E_L). Conversely, δ_C is -1 if component C is a sink term (ocean sink S_O, land sink S_L, cement carbonation S_C) or the atmospheric growth rate (G_A), assuming these sink/growth values are positive numbers in the component data. The term $(C_{23} - C_{17})$ represents the change in the estimate of component C between the two reports.

Data availability

The carbon budget component and imbalance data used in this study are sourced from the Global Carbon Budget papers[7,8]. The CAMS flux inversion data can be accessed from the following URL: www.ecmwf.int/en/forecasts/dataset/cams-greenhouse-gas-ghg-flux-inversions (last access 29 July 2024). The Jena CarboScope (CS) flux inversion data are available at: www.bgc-jena.mpg.de/CarboScope/ (last access 29 July 2024).

References

1. Schimel, D. S. & Carroll, D. Carbon cycle–climate feedbacks in the post-Paris world. *Annu. Rev. Earth Planet. Sci.* **52**, 16.1–16.27 (2024).
2. Jones, C. D. et al. RECCAP2 future component: consistency and potential for regional assessment to constrain global projections. *AGU Adv.* **4**, e2023AV001024 (2023).
3. Peters, G. P. et al. Towards real-time verification of CO2 emissions. *Nat. Clim. Chang.* **7**, 848–850 (2017).
4. Sitch, S. et al. Trends and drivers of terrestrial sources and sinks of carbon dioxide: an overview of the TRENDY project. *Glob. Biogeochem.* **35**, 1–25 (2024).
5. Xi, F. et al. Substantial global carbon uptake by cement carbonation. *Nat. Geosci.* **9**, 880–883 (2016).
6. Hall, B. D. et al. Revision of the world meteorological organization global atmosphere watch (WMO/GAW) CO2 calibration scale. *Atmos. Meas. Tech.* **14**, 3015–3032 (2021).
7. Friedlingstein, P. et al. Global carbon budget 2023. *Earth Syst. Sci. Data* **15**, 5301–5369 (2023).
8. Le Quéré, C. et al. Global carbon budget 2017. *Earth Syst. Sci. Data* **10**, 405–448 (2018).
9. Humphrey, V. et al. Sensitivity of atmospheric CO2 growth rate to observed changes in terrestrial water storage. *Nature* **560**, 628–631 (2018).
10. Pandey, S. et al. Toward low-latency estimation of atmospheric CO2 growth rates using satellite observations: evaluating sampling errors of satellite and in situ observing approaches. *AGU Adv.* **5**, e2023AV001145 (2024).
11. Masarie, K. A. & Tans, P. P. Extension and integration of atmospheric carbon dioxide data into a globally consistent measurement record. *J. Geophys. Res.* **100**, 11593–11610 (1995).
12. Ballantyne, A. P., Alden, C. B., Miller, J. B., Tans, P. P. & White, J. W. C. Increase in observed net carbon dioxide uptake by land and oceans during the past 50 years. *Nature* **488**, 70–73 (2012).
13. Rigby, M. et al. Role of atmospheric oxidation in recent methane growth. *Proc. Natl Acad. Sci. USA* **114**, 5373–5377 (2017).
14. Cunnold, D. M. et al. Global trends and annual releases of CCl3F and CCl2F2 estimated from ALE/GAGE and other measurements from July 1978 to June 1991. *J. Geophys. Res. Atmos.* **99**, 1107–1126 (1994).
15. Georgii, H. W. & Jost, D. Concentration of CO2 in the upper troposphere and lower stratosphere. *Nature* **221**, 1040 (1969).
16. Chevallier, F., Lloret, Z., Cozic, A., Takache, S. & Remaud, M. Toward high-resolution global atmospheric inverse modeling using graphics accelerators. *Geophys. Res. Lett.* **50**, e2022GL102135 (2023).
17. Rödenbeck, C., Zaehle, S., Keeling, R. & Heimann, M. How does the terrestrial carbon exchange respond to inter-annual climatic variations? a quantification based on atmospheric CO2 data. *Biogeosciences* **15**, 2481–2498 (2018).
18. Mercado, L. M. et al. Impact of changes in diffuse radiation on the global land carbon sink. *Nature* **458**, 1014–1017 (2009).
19. O'Sullivan, M. et al. Aerosol-light interactions reduce the carbon budget imbalance. *Environ. Res. Lett.* **16**, 125005 (2021).
20. Bakker, D. C. E. et al. A multi-decade record of high-quality fCO2 data in version 3 of the surface ocean CO2 Atlas (SOCAT). *Earth Syst. Sci. Data* **8**, 383–413 (2016).
21. Friedlingstein, P. et al. Global carbon budget 2021. *Earth Syst. Sci. Data* **14**, 1917–2005 (2022).
22. Friedlingstein, P. et al. Global carbon budget 2020. *Earth Syst. Sci. Data* **12**, 3269–3340 (2020).
23. Crippa, M. et al. *Fossil CO2 and GHG Emissions of all World Countries*. https://edgar.jrc.ec.europa.eu/report_2019 (2019).
24. CarboScope. *Jena CarboScope*. https://www.bgc-jena.mpg.de/CarboScope/ (2024).
25. Lan, X. et al. *Atmospheric Carbon Dioxide Dry Air Mole Fractions from the NOAA GML Carbon Cycle Cooperative Global Air Sampling Network*. https://doi.org/10.15138/wkgj-f215 (2025).
26. Baier, B., Sweeney, C., Newberger, T., Higgs, J. & Wolter, S. *NOAA AirCore Atmospheric Sampling System Profiles*. https://doi.org/10.15138/6AV0-MY81 (2021).

Acknowledgements

Part of this work was carried out at the Jet Propulsion Laboratory, California Institute of Technology, under a contract with the National Aeronautics and Space Administration (80NM0018D0004). We acknowledge discussions with Dr. David Schimel, Jet Propulsion Laboratory, California Institute of Technology, Pasadena, CA, USA.

Author contributions

S.P. conceptualized the study and performed the analysis. F.C. and C.R. provided the flux inversion data. S.P., C.F., B.B., J.L., and A.C. discussed the results, guided the analysis, and wrote the manuscript with comments from all authors.

Competing interests

The authors declare no competing interests.

Additional information

Supplementary information The online version contains supplementary material available at https://doi.org/10.1038/s41467-025-61588-2.

Correspondence and requests for materials should be addressed to Sudhanshu Pandey.

Peer review information *Nature Communications* thanks Christine Delire, Rachel Law and the other, anonymous, reviewer(s) for their contribution to the peer review of this work. A peer review file is available.